Iraqi Journal of Physics, 2023 *Vol. 21, No.2, PP. 91-98*

https://doi.org/10.30723/ijp.v21i2.1120

P-ISSN: 2070-4003
E-ISSN: 2664-5548

D-Shaped Photonic Crystal Fiber Toxic Metal Ions (Arsenic) Sensor Based on Surface Plasmon Resonance

Ghufran Mohammed Jassam[1a]* and Soudad S. Ahmed[1b]
[1]*Department of Physics, College of Science, University of Baghdad, Baghdad, Iraq*
[b]E-mail: soudadbassam@gmail.com
[a*]Corresponding author: ghofran.mohammed1104a@sc.uobaghdad.edu.iq

Abstract

In this work, a Photonic Crystal Fiber (PCF) sensor based on the Surface Plasmon Resonance (SPR) technology was proposed. A thin layer of gold (Au) was deposited on a D-shaped Photonic Crystal Fiber (PCF), which was coated with plasmonic chemically stable gold material with a thickness of 40nm. The performance parameters like sensitivity including wavelength sensitivity and amplitude sensitivity and resolution were evaluated by simulation using COMSOL software. The proposed sensor was created by using the finite element approach, it is numerically examined. The results show that the surface of D-shaped Photonic Crystal Fiber coated with Au behaves as a sensor to detect the refractive index (IR) of toxic metal ions. The impacts of the structural characteristics on the resonant spectra are also researched in order to improve sensing performance. The greatest amplitude sensitivity S_A was 99.2 RIU^{-1} and maximum resolution was 4 x 10^{-5} RIU achieved within the detection range (1.351-1.363).

Article Info.

Keywords:
Surface Plasmon Resonance, Optical Fiber Sensor, Toxic Metal Ions in Water, Photonic Crystal Fiber, D-shaped PCF

Article history:
Received: Apr. 06, 2023
Accepted: May 15, 2023
Published: Jun. 01,2023

1. Introduction

The advancements in fiber manufacturing technology over the past 20 years have been essential for optical fiber communications and other optical devices of high performance. PCFs have received a lot of interest in recent years due to their unique features that are not attained in traditional optical fibers, such as their small size, which reduces electromagnetic interference, as well as their high sensitivity, electrical passiveness, improved stability, and fast optical response [1]. Unlike conventional optical fibers, photonic crystal fiber has special properties, including low dispersion, high reflectivity, and low nonlinearity. All these features are a result of its unique design, which involves continually enhancing single-mode confinement by putting a string of air-filled holes along the PCF's length [2]. PCF sensors are based on surface plasmon propagation. They are widely used to monitor refractive index because of their super sensitivity, easy integration, fast response, and instant results.

PCFs are divided into two categories depending on their light-guiding mechanisms: Solid Core Photonic Crystal Fibers (SC-PCFs), which use Modified Total Internal Reflection (MTIR) and Hollow Core Photonic Crystal Fibers (HC-PCFs), which use the Photonic Band Gap (PBG) effect [3, 4].

Surface Plasmon Resonance (SPR) is defined as an optical phenomenon that occurs when p-polarized light excites a charge density oscillation at the metal-dielectric interface by achieving the phase-matching state between the p-polarized light and SP [5-9]. Combining the advantages of PCF technology with plasmonic science, PCF-SPR sensors have been developed for a wide range of potential applications such as water testing [10], food safety, solution concentration measurement [11], environmental

monitoring, biochemistry research [12], gas detection, medical diagnostics, and so on [13].

The sensing mechanism of PCF-SPR is achieved by means of an evanescent field. When light of a specific wavelength is incident on the fiber core of the PCF, and some fields pass into the cladding, an evanescent field is formed. When evanescent fields interact with free electrons in a plasmonic metal layer like silver, gold, copper, or aluminum, a surface plasmon wave is created. The core guided and SPP modes are now coupled, and the core guidance mode's RI (real value) is similar to that of the SPP mode, known as phase matching [14, 15].

PCF-SPR technology overcomes conventional prism-based SPR sensing challenges, including bulky construction, an accurate incident angle, and many moving mechanical components, which limit remote sensing and a broad range of applications [16]. There are two types of sensing approaches based on sensor evaluation: internal and external. The analyte is used to fill the air hole in the internal sensing or nanowire-based sensing, or a metal layer is coated around the core. Placing the plasmonic material externally is another approach to external sensing media, such as microchannel sensors, slit sensors, and D-shape [17].

Rifat et al. investigated an internally metal-coated PCF as an SPR sensor with a wavelength sensitivity (S_W) of 300 nm/RIU and an amplitude sensitivity (S_A) of 418 RIU^{-1} within a sensing range of 1.46–1.49 RIU [18]. They improved the sensitivity and detection range of the internally coated sensor by introducing a bigger cavity inside the fiber core [19]. Mahmood et al. proposed a PCF-SPR sensor with a maximum sensitivity of 164.3 nm/RIU in the sensing range of analyte RI 1.33–1.3431. They used a plasmonic material, such as gold, to coat the air holes, which they filled with an analyte samples [20].

In this study, however, sensor performance was significantly improved by using an internal sensing approach. As a result, effective coupling was obtained between the core-guiding mode and the SPP mode, improving the sensor's performance. Most of the reported PCF conformations were difficult to fabricate because of their small air hole diameter, complicated structure, and small fiber diameter. Most demonstrated PCF-SPR sensors have been mathematically investigated, and the finite element method (FEM) was used to investigate ESM-12-02 based on SPR. The fabricated PCF consists of a solid core surrounded by a periodic array of six air holes. The over side of the D-shape of the PCF solid core was chosen, coated with a chemically stable material, such as gold, and filled with an analyte. The proposed structure can achieve maximum sensitivity, including amplitude sensitivity and sensor resolution. The proposed design was extremely sensitive, making it an excellent component for detecting toxic metal ions in water and determining water quality.

2. Theoretical Model

2.1. Sellmeier Equation

Silica is mostly employed in the fabrication of the suggested sensor. The holes are all empty, i.e., filled with air. The refractive index (RI) is calculated using Eq. (1) [21]:

$$N_{silica} = 1 + \frac{a_1\lambda^2}{\lambda^2 - b_1} + \frac{a_2\lambda^2}{\lambda^2 - b_2} + \frac{a_3\lambda^2}{\lambda^2 - b_3} \quad (\mathbf{1})$$

where: N is the refractive index of silica, which changes depending on the wavelength, λ is the wavelength, and Sellmeier coefficients are (a_1, a_2, a_3) and (b_1, b_2, b_3), where a_1=0.6961663, a_2=0.4079426, a_3= 0.8974794, b_1=0.0684043 μm^2, b2= 0.1162414 μm^2 and b_3=9.896161 μm^2.

2.1. Confinement Losses (L_C)

Confinement loss (L_C) is a form of loss that occurs in PCFs and reflects the light confinement ability within the core region. When the optical mode propagates in the core region, one must take into consideration that the number of layers of air-holes is finite and light leaking from the core to the exterior material occurs through the bridges between the air-holes, resulting in confinement loss. L_C in units of dB/km, is calculated using Eq. (2) [22]:

$$L_c = \frac{2\pi\left(\frac{20}{\ln 10}\right)\mathrm{Im}(n_{eff})}{\lambda} = 8.686\frac{2\pi}{\lambda}\,\mathrm{Im}(n_{eff}) \qquad (2)$$

where: $\mathrm{Im}(n_{eff})$ is the imaginary part of the refractive index and (λ) is the wavelength. The confinement loss decreases exponentially by increasing the number of rings of cladding air holes, and is determined by the geometry of the structure.

3. Photonic Crystal Fiber for Endlessly Single Model (ESM-12-02)

The Single Mode Solid Core Photonic Crystal Fiber is a typical PCF, Endlessly Single Mode (ESM-12-02) (supplied by Thorlabs Company) exhibits minimal loss throughout the broadest wavelength range (200 nm to above 2000 nm) while maintaining a nearly constant mode field diameter. The ESM-12-02 is compatible with all popular fiber tools and has a standard 125 m outside diameter. ESM-12-02 was utilized to produce broadband radiation in a single spatial mode for sensors, interferometers, and short-wavelength applications (visible light and UV). Table 1 lists the ESM-12-02 physical characteristics. Fig. 1 shows a scanning electron microscope (SEM) image of (ESM-12-02) PCF with a lattice constant (Λ) of 7.8 μm and an air hole diameter (d) of 4.5 μm.

Table 1: Physical Properties of ESM-12.

Physical Properties	
Core measurement	12.2 μm
OD, or outer cladding diameter	125 μm
Size of the coating	245 μm
cladding and core materials	Pure silica
single-layer coating material	Acrylate
Continuity of the coating	< 10 μm
Proving level	0.5 %

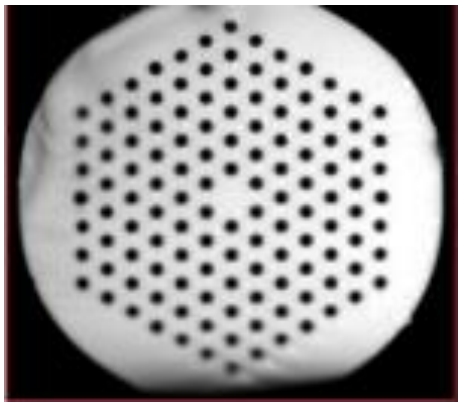

Figure 1: SEM image OF PCF.

4. Structure Design and Analysis

The photonic crystal fiber (PCF) model (ESM-12) made by NKT Photonics has always been an endless single mode fiber with an outer diameter of 125 µm. It is compatible with all common fiber tools. Fig. 2 shows a schematic diagram of the proposed PCF-SPR sensor, which was created using the COMSOL MULTPHYSICS software. The analyte was filled over a D-shape PCF, which was coated with a 40 nm thick layer of plasmonic material such as gold. A Perfectly Matched Layer (PML) was used as the boundary media to absorb the scattering light toward the fiber surface. PML, in the proposed structure, is a circular layer with a thickness of 12 µm. Convergence tests were also successfully completed, and optimized with the PML thickness and mesh size for more accurate results.

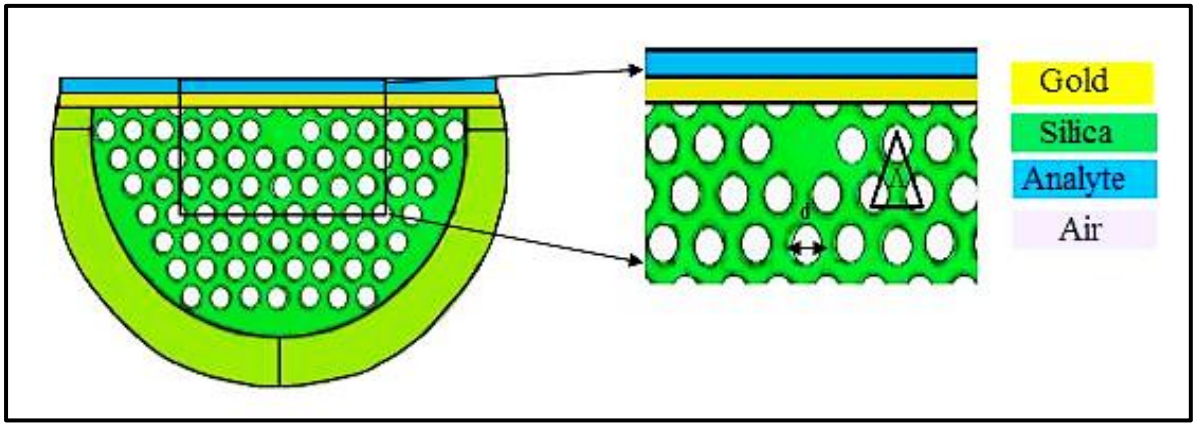

Figure 2: Cross section views of D-shape PCF.

5. Results and Discussion

For a certain sample, resonance is produced at a given wavelength by phase matching between the Surface Plasmon Polariton (SPP) mode and core guiding. The dispersion relation between the second surface plasmon polariton (SPP) mode and the fundamental mode for the y-polarizations around the resonant frequency is depicted in Fig. 3c. This graphic also displays the confinement loss of the structure's overall propagation mode (red line). There was a significant loss peak where the core directed the 2nd surface plasmon polariton mode and crossed at the resonant wavelength λ_{res} of 630 nm. As a result, the SPP mode receives the greatest energy from the basic core mode. Fig. 3 also displays the electrical-filed distribution for the (a) basic core-guiding mode and (b) phase matching core mode in the y-polarization.

These results were obtained using a phase-matching condition and a refraction index of 1.363 for the analyte. The loss depth was greatly influenced by small changes in the analyte refractive index (RI). The proposed PCF sensor's loss spectrum with different n_a is displayed in Fig. 4. As the loss depth increased, the peak shifted toward longer wavelengths (redshift). This is because an increased effective refractive index (n_{eff}) of the surface plasmon mode modulates the phase matching point, reducing the difference between core guided mode and plasmon mode, making the coupling efficiency stronger. For n_a =1.363 at 630 nm, the maximum loss depth occurred and was equal to 41 dB/ cm. The power exchange between the core and SPP modes increased with the increase in loss depth, owing to an increase in the RI of the analyte, resulting in a narrow resonant spectrum.

(a) (b)

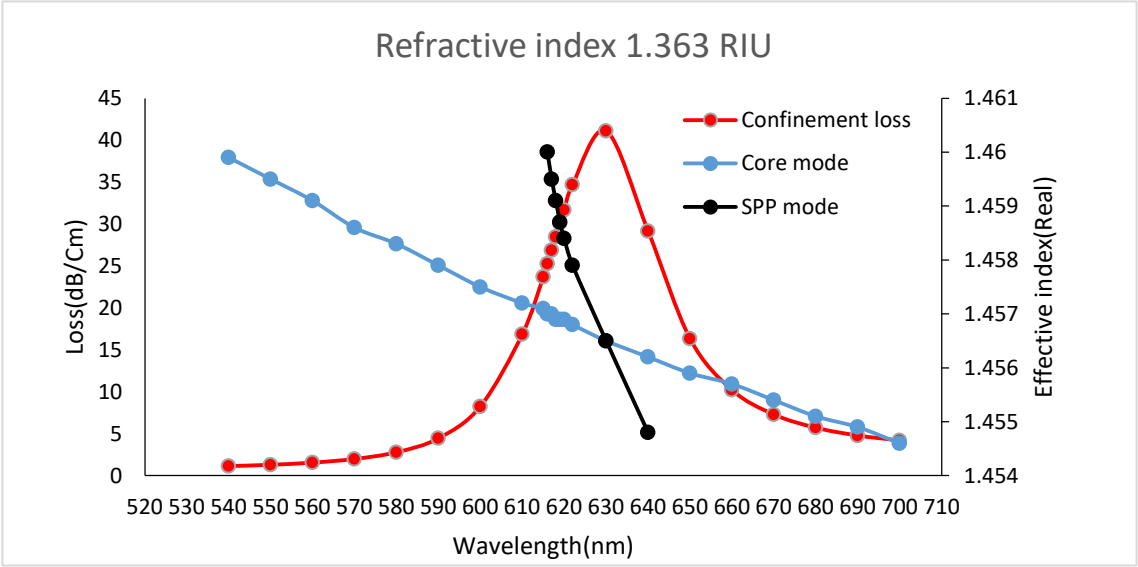

(c)

Figure 3: Electric field distributions at n_a =1.3624 in (a) core-guided mode, (b) condition of phase-matching, (c)dispersion relation between core guiding mode and the second Surface plasmon mode.

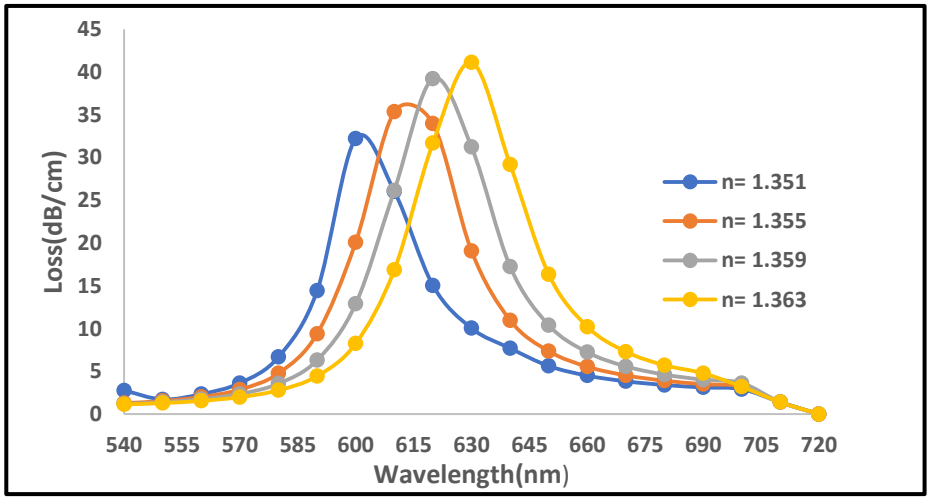

Figure 4: The confinement loss spectrum of the proposed PCF SPR sensor variation with increase analyte RI from 1.351 to 1.363.

Both amplitude interrogation and wavelength methods can be used to assess the suggested sensor's performance. Eq. (3) may be used to compute the wavelength sensitivity [23]:

$$S_W(\lambda) = \frac{\Delta\lambda_{peak}}{\Delta n_a} \quad (3)$$

$\Delta\lambda_{peak}$ and Δn_a indicate the change in the resonant peaks and the analyte refractive index, respectively.

For refractive index (n_a) of 1.351, 1.355, and 1.359, the proposed sensor has wavelength sensitivity of 2500 nm/RIU. The peaks of resonant wavelength are 10 nm, for analyte refractive index variations of 1.351–1.355, 1.355–1.359, and 1.359-1.363 represent the distance between the peaks of resonant wavelength. Another important parameter is the sensor's resolution which describes how the sensor detects a small change in the analyte RI. Resolution (R) of the proposed sensor was given by Eq. (4) [24]:

$$R = \frac{\Delta na \times \Delta\lambda min}{\Delta\lambda peak} \text{ [RIU]} \quad (4)$$

where: n_a is the variation in analyte\sample refractive index RI, $\Delta\lambda_{min}$ is the lowest spectral resolution and $\Delta\lambda_{peak}$ is the maximum resonant wavelength peak shift. The maximum resolution was 4×10^{-5} RIU, assuming $\Delta n_a = 0.004$, $\Delta\lambda_{min}= 0.1$, $n_a =1.363$ and $\Delta\lambda_{peak}= 10$ nm. Eq. (5) can be applied to determine the amplitude sensitivity of the sensor [18]:

$$S_A(\lambda) = -\frac{1}{\alpha(\lambda,n_a)}\frac{\partial\alpha(\lambda,n_a)}{\partial n_a} [RIU^{-1}] \quad (5)$$

where: $\alpha(\lambda, n_a)$ indicates the analyte's confinement loss L_C at a certain refractive index and $\partial\alpha(\lambda, n_a)$ represents the variation in confinement loss L_C between two analyte/sample with nearby refractive indices. Fig. 5 illustrates the amplitude sensitivity of different analyte/sample refractive indices. The highest possible amplitude sensitivity was 55.69 RIU^{-1}, 73.86 RIU^{-1}, and 99.2 RIU^{-1} when the analyte/sample refractive index variation range was 1.351-1.355, 1.355-1.359, and 1.359-1.363, respectively.

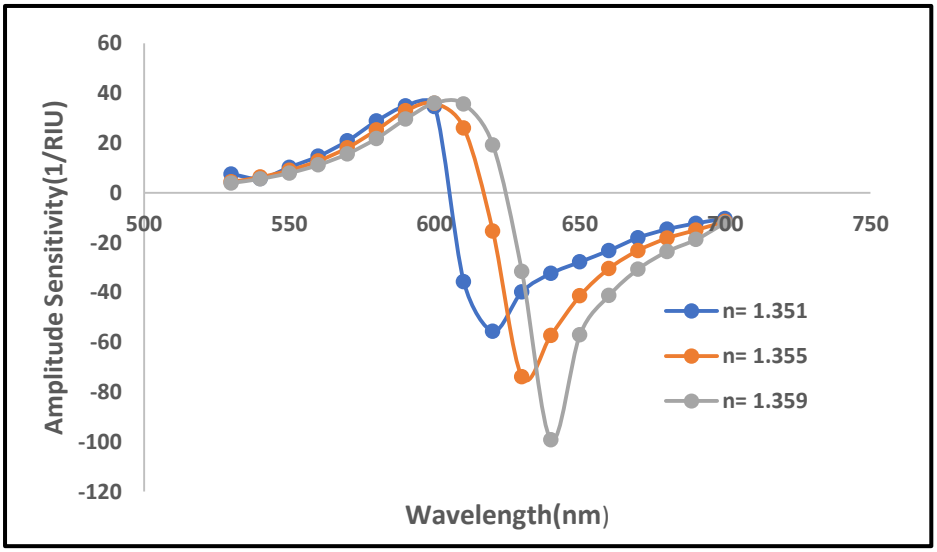

Figure 5: Amplitude sensitivity in relation to wavelength when the sample refractive index RI n_a rises from 1.351 to 1.36.

6. Conclusions

A toxic metal ion sensor based on the surface plasmon resonance technique was presented using photonic crystal fiber (PCF). There was a significant confinement loss in the y-polarization direction when the surface of the PCF core was coated with gold and then filled with a sample of toxic metal ions in water. When the SPR sensor's resonant wavelength matches the resonant wavelength λ_{res} or the peak of the transmission loss spectrum, the filled analyte may be detected. The fundamental mode sensor parameters were investigated using the finite element method (FEM). The amplitude sensitivity of 99.2 RIU^{-1} and the maximum resolution of $4x10^{-5}$ RIU were obtained in the sensing range of 1.351 (nickel toxic metal ions in water) to 1.363 (arsenic toxic metal ions). This detector, due to its high sensitivity, is recommended for use in environmental monitoring for chemical and biological sensing applications, such as detecting heavy metals in water.

Acknowledgements

The authors would like to thanks the University of Baghdad, Collage of Science, Department of Physics, for assist us in this article.

Conflict of interest

Authors declare that they have no conflict of interest.

References

1. M. Khatun, M. Islam, and A. Bazlur Rashid, Comput. Eng. Intell. Sys. **3**, 1 (2012).
2. M. A. Islam, M. R. Islam, A. M. Al Naser, F. Anzum, and F. Z. Jaba, J. Comput. Elect. **20**, 377 (2021).
3. R. Gupta, F. Rahi Alhachami, I. Khalid, H. S. Majdi, N. Nisar, Y. Mohamed Hasan, R. Sivaraman, R. M. Romero Parra, Z. I. Al Mashhadani, and Y. Fakri Mustafa, Crit. Rev. Anal. Chem. **0**, 1 (2022).
4. E. Podder, M. B. Hossain, R. H. Jibon, A. a.-M. Bulbul, and H. S. Mondal, Front. Optoelect. **12**, 372 (2019).
5. G. M. Jassam, Iraqi J. Phys. **17**, 11 (2019).
6. N. S. Rahim, S. S. Ahmed, and M. F. Sultan, Iraqi J. Sci. **61**, 1650 (2020).
7. E. Khatar and S. S. Bassam, Iraqi J. Phys. **19**, 51 (2021).
8. N. S. Rahim, Iraqi J. Phys. **17**, 41 (2019).
9. G. M. Jassam, S. S. Alâ, and M. F. Sultan, Iraqi J. Sci. **61**, 765 (2020).
10. N. Muhammed, A. Mahmood, S. A. Kadhim, and I. Naseef, J. Phys.: Conf. Ser. (IOP Publishing, 2020). p. 012134.
11. S. Maheswaran, P. Kuppusamy, S. Ramesh, T. Sundararajan, and P. Yupapin, Resul. Phys. **11**, 577 (2018).
12. K. Ahmed, B. K. Paul, B. Vasudevan, A. N. Z. Rashed, R. Maheswar, I. Amiri, and P. Yupapin, Resul. Phys. **12**, 2021 (2019).
13. H. Yuan, W. Ji, S. Chu, Q. Liu, S. Qian, J. Guang, J. Wang, X. Han, J.-F. Masson, and W. Peng, ACS Sens. **4**, 704 (2019).
14. A. K. Paul, OSA Contin. **3**, 2253 (2020).
15. M. Li, J. Xu, Q. Zheng, C. Guo, and Y. Chen, Analyt. Chem. **94**, 7238 (2022).
16. M. T. Rahman, S. Datto, and M. N. Sakib, OSA Contin. **4**, 1808 (2021).
17. A. A. Rifat, M. R. Hasan, R. Ahmed, and H. Butt, J. Nanophot. **12**, 012503 (2018).
18. A. A. Rifat, G. A. Mahdiraji, D. M. Chow, Y. G. Shee, R. Ahmed, and F. R. M. Adikan, Sensors **15**, 11499 (2015).
19. A. A. Rifat, F. Haider, R. Ahmed, G. A. Mahdiraji, F. M. Adikan, and A. E. Miroshnichenko, Opt. lett. **43**, 891 (2018).

20. A. I. Mahmood, R. K. Ibrahim, A. I. Mahmood, and Z. K. Ibrahim, J. Phys.: Conf. Ser. (IOP Publishing, 2018). p. 012118.
21. W. Sellmeier, Annal. der Phys. Chem. **219**, 272 (1871).
22. G. Agrawal, *Nonlinear Fiber Optics*. 5th Ed. (UK, USA, Elesevier, Academic Press, 2001).
23. G. Wang, S. Li, G. An, X. Wang, Y. Zhao, W. Zhang, and H. Chen, Opt. Quant Elect. **48**, 1 (2016).
24. A. A. Rifat, G. A. Mahdiraji, Y. M. Sua, R. Ahmed, Y. Shee, and F. M. Adikan, Opt. Expre. **24**, 2485 (2016).

مستشعر أيونات المعادن السامة (الزرنيخ) بالألياف البلورية الضوئية على شكل D على اساس رنين البلازمون السطحي

غفران محمد جسام[1] وسؤدد سلمان البصام[1]

[1] قسم الفيزياء، كلية العلوم، جامعة بغداد، بغداد، العراق

الخلاصة

في هذا العمل ، تم اقتراح متحسس من الألياف البلورية الضوئية (PCF) يعتمد على تقنية رنين البلازمون السطحي (SPR) . لترسيب طبقة رقيقة من الذهب على الألياف البلورية الضوئية على شكل حرف D . تم طلاء سطح من الألياف البلورية الضوئية على شكل D بسمك مادة ذهبية مستقرة كيميائياً من 40 نانومتر وتم تقييم معلمات الأداء مثل الحساسية تشمل حساسية الطول الموجي وحساسية السعة والدقة باستخدام المحاكاة باستخدام برنامج كومسول يتم إنشاء المستشعر المقترح ، وباستخدام نهج العناصر المحدودة ، يتم فحصه عدديًا.أظهرت النتائج أن أن سطح الألياف البلورية الضوئية على شكل D المطلي بـ الذهب تتصرف كمستشعر للكشف عن معامل انكسار أيونات المعادن السامة في الماء .يتم أيضًا البحث في تأثيرات الخصائص الهيكلية على أطياف الرنين من أجل تحسين أداء الاستشعار.كانت حساسية السعة الأكبر هي $99.2\ RIU^{-1}$ وكانت الدقة القصوى 4×10^{-5} RIU تم تحقيقها داخل نطاق الكشف 1.351-1.363.

الكلمات المفتاحيه: رنين البلازمون السطحي، متحسس الليف البصري، أيونات المعادن السامة في الماء، الألياف الكريستالية الضوئية، الألياف الكريستالية الضوئية على شكل حرف D .